JGR Atmospheres

RESEARCH ARTICLE
10.1029/2024JD041902

Key Points:
- Advective transport between the stratosphere and mesosphere exhibits a robust annual cycle
- Models project an average amplification of cross-stratopause transport of about 1% per decade during all seasons
- The transport decomposition reveals inconsistencies between the models regarding the causes of long-term changes

Supporting Information:
Supporting Information may be found in the online version of this article.

Correspondence to:
P. Šácha,
petr.sacha@matfyz.cuni.cz

Citation:
Zajíček, R., Mikšovský, J., Eichinger, R., Pišoft, P., & Šácha, P. (2024). Advective transport between the stratosphere and mesosphere. *Journal of Geophysical Research: Atmospheres*, *129*, e2024JD041902. https://doi.org/10.1029/2024JD041902

Received 1 JUL 2024
Accepted 16 NOV 2024

Author Contributions:
Conceptualization: R. Zajíček, P. Šácha
Data curation: R. Eichinger
Formal analysis: R. Zajíček
Funding acquisition: R. Zajíček, P. Šácha
Investigation: R. Zajíček
Methodology: R. Zajíček, P. Šácha
Project administration: P. Šácha
Software: R. Zajíček
Supervision: P. Šácha
Visualization: R. Zajíček, J. Mikšovský
Writing – original draft: R. Zajíček, P. Šácha
Writing – review & editing: J. Mikšovský, R. Eichinger, P. Pišoft, P. Šácha

Advective Transport Between the Stratosphere and Mesosphere

R. Zajíček[1], J. Mikšovský[1], R. Eichinger[1,2], P. Pišoft[1], and P. Šácha[1]

[1]Department of Atmospheric Physics, Faculty of Mathematics and Physics, Charles University, Prague, Czech Republic,
[2]Deutsches Zentrum für Luft- und Raumfahrt (DLR), Institut für Physik der Atmosphäre, Weßling, Germany

Abstract The Brewer-Dobson circulation (BDC) characterizes the large-scale meridional overturning mass circulation influencing the composition of the whole middle atmosphere. The BDC consists of two separate parts—a shallow branch in the lower stratosphere and a deep branch higher in the middle atmosphere. Climate models robustly project the advective BDC part to accelerate due to greenhouse gas-induced climate change and this acceleration strongly influences middle atmospheric chemistry and physics in the projections. A prominent quantity that is being studied as a proxy for advective BDC changes is the net tropical upwelling across pressure levels, particularly in the lower stratosphere. The upper branch of the BDC has received considerably less research attention than its shallow part, although, together with the mean mesospheric pole-to-pole circulation, it couples the stratosphere and mesosphere and is responsible for a large portion of the interhemispheric transport in the middle atmosphere. Aiming to fill this gap, we here study climatology and trends in advective mass transport across the stratopause. Results based on the analysis of seven CCMI models include quantification of the climatological cross-stratopause advective transport, characterization of its interannual variability and long-term trend as well as detailed analysis of inter-model differences using a novel decomposition methodology. Our results demonstrate that the changes in circulation speed as well as changes in horizontal and vertical structure in the upper stratosphere and mesosphere jointly shape the projected increasing advective mass flux across the stratopause due to increasing greenhouse-gas emissions.

Plain Language Summary The Brewer-Dobson circulation (BDC) is an important circulation pattern, affecting the composition of the entire middle atmosphere. Our study focuses on the less-studied higher part of the BDC, which connects the stratosphere and mesosphere. Analyzing comprehensive climate model simulations, we found changes in circulation speed, along with horizontal and vertical structure changes of the upper BDC branch as a response to increasing greenhouse gas emissions. Understanding these changes aids improvements of climate predictions and highlights the significant influence of human activities on the atmosphere.

1. Introduction

The existence of a mean meridional global mass circulation in the middle atmosphere was originally anticipated based on the observed distributions of ozone (Dobson et al., 1929) and water vapor (Brewer, 1949). Nowadays, the so-called Brewer-Dobson circulation (BDC) is used more generally to characterize the features of the mean meridional mass transport influencing the overall composition of the whole middle atmosphere (Andrews et al., 1987). The BDC consists of two separate parts - shallow branches in the lower stratosphere of each hemisphere and a deep branch higher in the middle atmosphere, forming a single pole-to-pole circulation cell from the summer to the winter hemisphere (Birner & Bönisch, 2011; Plumb, 2002). The analytical model of the BDC is usually defined as consisting of a diffusive part, and an advective part described using the residual mean circulation (Dietmüller et al., 2017; Garny et al., 2014). Climate model simulations robustly show that the net mass transport by BDC increases in connection with the greenhouse gas (GHG)-induced climate change (Eichinger et al., 2019; Palmeiro et al., 2014; Shepherd & McLandress, 2011), and this increase dominates the middle atmospheric changes in climate model projections (Butchart, 2014). For historical BDC trends, ozone-depleting substances (ODSs) have been identified as a major forcing as well (Garcia, 2021).

Underlying this, anthropogenic emissions have a direct influence on the temperature and other state variables. There is robust observational evidence that the troposphere is warming, and the stratosphere is cooling in response to the radiative forcing of anthropogenic GHG emissions (IPCC, 2023), which affects the structure of the atmosphere. Following simple thermodynamical arguments, changes in the vertical structure of the atmosphere are inevitable and are being both robustly observed and simulated by the models (Berger & Lübken, 2011; Eichinger & Šácha, 2020; Laštovička, 2006; Pišoft et al., 2021; Santer et al., 2003). Moreover, the horizontal structure of the atmosphere is also changing (Hardiman et al., 2014; Staten et al., 2018). The overall BDC changes resulting from these structural modifications of the atmosphere are subject of current research (e.g., Oberländer-Hayn et al., 2016; Stiller et al., 2017; Šácha et al., 2019, 2024). Focusing on the advective part of the circulation, a prominent quantity that is being studied as a proxy for the BDC strength is the net tropical upwelling at 100 and 70 hPa, but also around 1 hPa for the deep branch of the BDC (Abalos et al., 2021; Palmeiro et al., 2014). The net upwelling measures the amount of mass advected across the isobar upwards by the residual mean circulation (note that for 1 hPa the upwelling region extends also outside of the tropics).

The mean meridional overturning circulation in the upper stratosphere and mesosphere has received less research attention than the shallow BDC branch but features some striking phenomena. Here, the deep BDC branch overlies with the pole-to-pole general circulation in the mesosphere (Smith, 2012) and together they control the exchange of air between the stratosphere and mesosphere, mediating also the interhemispheric transport. Over the summer pole, the circulation consists of rising air that adiabatically cools the mesosphere resulting in extremely low temperatures that allow formation of polar mesospheric clouds in the summer polar regions (Olivero & Thomas, 1986; Thomas, 1991). Conversely, at the winter pole, the downwelling air adiabatically heats the middle atmosphere (Karlsson et al., 2007). During the process, the circulation modulates the vertical structure of the stratosphere and mesosphere at both poles (and therefore the location of the stratopause) and contributes to the dynamical interhemispheric coupling in the upper stratosphere (Smith et al., 2020) and to some extent possibly also in the mesosphere (Smith et al., 2022).

The deep branch of the BDC has been found to accelerate in climate model projections (Lin & Fu, 2013). However, no effort has been made to date to quantify how this affects the stratosphere-mesosphere exchange, that is, the amount of mass flux crossing the stratopause. The motivation for studying this aspect of the mean meridional circulation in the middle atmosphere is underlined by its connection with many vivid research questions. In the circulation direction from the mesosphere to the stratosphere, there is a growing interest in the downward transport of mesospheric metals (Plane et al., 2015), including aluminum, from meteors and satellite re-entry and launching, with frequencies of the latter two expected to increase considerably in the near future (D'Ambrosio et al., 2022). Another important aspect is the wintertime transport of NO_x from the mesosphere to the stratosphere, which has implications for ozone variability via the catalytic NO_x cycle. NO_x is primarily produced in the upper atmosphere through energetic electron precipitation (Andersson et al., 2018) and sporadic solar proton events (Jackman et al., 2008). In winter, the absence of photolysis and the longer lifetime of NO_x enables its transport to the stratosphere. Moreover, vertical winds in the mesosphere can be estimated from the descent of NO_x mixing ratio isolines (Orsolini et al., 2017).

In the opposite direction, the importance of transport from the stratosphere to the mesosphere has been recently linked with the uncertainty of stratospheric age of air and therefore BDC strength estimates based on SF_6 trace gas concentrations (Garny et al., 2024). This is due to the role of previously unaccounted mesospheric SF_6 sinks for the estimates (Loeffel et al., 2022; Ray et al., 2017). Additionally, many studies focus on stratospheric trace gas budgets. This is of particular importance for water vapor (e.g., Brinkop et al., 2016; Solomon et al., 2010) and ozone (e.g., Ball et al., 2017; Steinbrecht et al., 2017). Discussions around these budgets typically focus on in situ formation and exchange with the troposphere, but a comprehensive understanding of stratospheric trace gas budgets also requires consideration of exchange with the mesosphere.

Addressing this research gap, we present a pioneering study quantifying the climatological advective transport across the stratopause as well as characterizing its annual and interannual variability and long-term trend. In doing so, we account for seasonal and long-term variability and trends of the stratopause itself, which is connected with the structural changes of the atmosphere. Moreover, we provide a detailed analysis of inter-model differences using a novel methodology for decomposing advective BDC changes into individual mechanisms introduced by Šácha et al. (2024).

The study is structured as follows. First, we describe the data and methods, especially the decomposition methodology and its interpretation. Then, we show the climatology of the cross-stratopause mass exchange, its seasonal variability and spatial structure. Next part of the paper is dedicated to long-term trends of cross-stratopause transport with a focus on inter-model differences revealed by the decomposition methodology.

Table 1
List of the Included CCMI-1 Models

Model	Top of model	No. of levels between 5 and 0.1 hPa	References
GEOSCCM	1 Pa	16	Molod et al. (2012, 2015)
			Oman et al. (2011, 2013)
NIWA-UKCA	84 km	12	Stone et al. (2016)
EMAC-L47MA	1 Pa	8	Jöckel et al. (2010, 2016)
EMAC-L90MA	1 Pa	25	Jöckel et al. (2010, 2016)
CMAM	0.0575 Pa	13	Jonsson et al. (2004)
			Scinocca et al. (2008)
ACCESS-CCM	84 km	12	Morgenstern et al. (2009, 2013)
MRI-ESM1r1	1 Pa	11	Deushi and Shibata (2011)
			Yukimoto et al. (2012)

Note. Full information about model references can be found in Morgenstern et al. (2017).

The paper concludes with a summary and discussion on the challenges and complexities of accurately projecting changes within the mean meridional overturning circulation in the upper stratosphere and mesosphere, emphasizing the significant impact of vertical and horizontal atmospheric structure changes and the need for better observational constraints to refine model predictions.

2. Data and Methodology

2.1. Data and Statistical Approach

We analyzed 7 global chemistry-climate model simulations (see Table 1), which contributed to the Chemistry Climate Model Initiative Phase 1 (CCMI-1) REF-C2 scenario (Morgenstern et al., 2017) and provided all the necessary data for the analysis. The REF-C2 simulations follow the A1 scenario for ODSs (World Meteorological Organization, 2011) and the RCP6.0 (Representative Concentration Pathway) scenario for other GHGs, tropospheric ozone precursors, and aerosol precursor emissions (Meinshausen et al., 2011). Anthropogenic emissions are based on MACCity (Granier et al., 2011) until 2000, followed by RCP 6.0 emissions.

We use monthly mean zonal mean temperature, geopotential height, and residual mean velocity components from the Transformed Eulerian Mean (TEM) framework, covering the period from 1960 to 2099 for each individual model. The stratopause height has been calculated on a monthly basis as the level of maximum temperature between 40 and 65 km.

Seasonal climatologies in the paper are based on monthly mean values. We consider the standard seasons: December–February (DJF), March–May (MAM), June–August (JJA), and September-November (SON). Linear temporal trends presented in this study were calculated using linear regression, with regression coefficients estimated by the ordinary least squares method.

2.2. Transport Across the Stratopause

To quantify cross-stratopause transport, we used the formula for the mass flux through a time-variable oriented zonal mean surface as defined in Šácha et al. (2024), which also allows for contributions from the meridional residual mean velocity components across the sloping stratopause. A separate analysis is performed for the transport from the stratosphere to the mesosphere (hereafter referred to as upward transport) and from the mesosphere to the stratosphere (downward transport). For this, boundaries (turn-around latitudes) of the upward and downward transport regions are first detected as the points with the zeroth mass flux across the stratopause. Note that the turn-around latitudes determined in this way do not match the commonly used turn-around latitudes based only on vertical mass flux. The net upward or downward transport is defined at a given time instance as an integral between the turn-around latitudes accordingly (φ_1 and φ_2 for a single domain for simplicity):

$$U = 2\pi a^2 \int_{\varphi_1}^{\varphi_2} \overline{\rho}(\overline{w}^* + \overline{v}^* \tan \alpha) \cos \varphi \, \mathrm{d}\varphi. \tag{1}$$

where U is the net zonal mean transport from the stratosphere to the mesosphere or reverse, a is the radius of the Earth, $\overline{\rho}$ is the zonal mean density, $\overline{w}^*$ (converted from $\mathrm{Pa} \cdot \mathrm{s}^{-1}$ to $\mathrm{m} \cdot \mathrm{s}^{-1}$) and $\overline{v}^*$ are the vertical and meridional residual mean velocities, and α is the slope of the zonal mean stratopause relative to the horizontal plane, which can be determined by simple trigonometry from the known zonal mean stratopause height meridional distribution. φ_1 or φ_2 could include the poles if the upward/downward transport region extends to them.

2.3. Decomposition Method

Šácha et al. (2024) showed that temporal changes expressed by Equation 1 can be at the leading order analytically decomposed into individual kinematic terms in the z-plane (z is taken as a geopotential height). This allows disentangling the contributions from the structural changes of the atmosphere and from the accelerating circulation to the net transport change. The exact form of the numerical implementation can be found in Šácha et al. (2024). The final and closed set of mechanisms contributing to the net upwelling or downwelling changes are:

1. Contribution from width changes of the upward/downward transport region (width term):

$$2\pi a^2 \int_{\varphi_2(t)}^{\varphi_2(t+\delta t)} \overline{\rho}(\overline{w}^* + \overline{v}^* \tan \alpha) \cos \varphi \, \mathrm{d}\varphi - 2\pi a^2 \int_{\varphi_1(t)}^{\varphi_1(t+\delta t)} \overline{\rho}(\overline{w}^* + \overline{v}^* \tan \alpha) \cos \varphi \, \mathrm{d}\varphi \tag{2}$$

2. Vertical shift effect (z term):

$$2\pi a^2 \int_{\varphi_1}^{\varphi_2} \frac{\partial \overline{z}}{\partial t} \frac{\partial \overline{\rho}(\overline{w}^* + \overline{v}^* \tan \alpha)}{\partial z} \cos \varphi \, \mathrm{d}\varphi \tag{3}$$

3. Vertical velocity acceleration ($\overline{w}^*$ term):

$$2\pi a^2 \int_{\varphi_1}^{\varphi_2} \overline{\rho} \frac{\partial \overline{w}^*}{\partial t} \cos \varphi \, \mathrm{d}\varphi \tag{4}$$

4. Meridional velocity acceleration ($\overline{v}^*$ term):

$$2\pi a^2 \int_{\varphi_1}^{\varphi_2} \tan \alpha \overline{\rho} \frac{\partial \overline{v}^*}{\partial t} \cos \varphi \, \mathrm{d}\varphi \tag{5}$$

5. Density contribution to the mass flux changes (ρ term):

$$2\pi a^2 \int_{\varphi_1}^{\varphi_2} (\overline{w} + \overline{v}^* \tan \alpha) \frac{\partial \overline{\rho}}{\partial t} \cos \varphi \, \mathrm{d}\varphi \cdot \delta t \tag{6}$$

6. Stratopause shape variations controlling the efficiency of the meridional transport (shape term):

$$2\pi a^2 \int_{\varphi_1}^{\varphi_2} \frac{\overline{\rho v}^*}{\cos^2\alpha} \frac{\partial \alpha}{\partial t} \cos\varphi \, d\varphi \quad (7)$$

In Equation 3, $\overline{z}$ refers to the zonal mean stratopause height.

This decomposition allows us to derive for each mechanism a time series of contributions to the changes in net upward or downward transport. Although the physical meaning of the individual decomposition terms is fully described in Šácha et al. (2024), it will be briefly explained in the following paragraphs with emphasis on the expected behavior of these terms in the case of transport through the stratopause.

$\overline{w}^*$ and $\overline{v}^*$ terms (Equations 4 and 5) involve a local tendency (at fixed z) of the residual circulation. Circulation can vary at a fixed geometric height by a combination of two processes: first, it can be accelerating in the Lagrangian sense, or second, as discussed in Oberländer-Hayn et al. (2016), circulation may show accelerating tendencies in some vertical coordinates (e.g., the z-frame) and remain fixed at others (e.g., isentropic or pressure levels). As the troposphere expands and the stratosphere and mesosphere cool (Mlynczak et al., 2022), isentropic levels shift vertically in the z-system. If there is an underlying vertical gradient of the circulation's velocity, local tendencies $\frac{\partial \overline{w}^*}{\partial t}$ and $\frac{\partial \overline{v}^*}{\partial t}$ can arise in the z-system even if the circulation following the isentropes remains unchanged. Here, the decomposition method works in the z-frame to reveal the portion of local tendencies that can be connected with such upward shifts. In our case, cross-stratopause transport changes connected with the changing stratopause height $\overline{z}$ with time are included in the z term (Equation 3). For this both the already discussed circulation gradient as well as climatological density gradient play a role. As the stratopause shifts downwards to a region of higher air density, this is evaluated in the z-frame as a contribution to the amplification of the mass transport and z term is expected to be positive.

As the upper stratosphere significantly cools, one might expect the cooling to further contribute to the increasing cross-stratopause transport through positive density tendency in the ρ term (Equation 6). However, pressure changes in the stratopause region have to be accounted for as well. Differentiating the ideal gas state equation yields $\frac{\partial \rho}{\partial t} = RT\frac{\partial p}{\partial t} - \frac{Rp}{T^2}\frac{\partial T}{\partial t}$, where T is the temperature, and R is the gas constant of dry air. The local pressure tendency is expected to be negative as pressure levels are moving downwards in the upper stratosphere (the stratopause loses pressure in an average sense), but the latter term involving a temperature tendency should be positive. Hence, the density tendency results from the sum of two opposing factors and taken together with the vertical shift effect, the behavior of the ρ term cannot be anticipated directly.

The width term (Equation 2) captures the effect of turn-around latitude position changes. For example, if the region where upward transport takes place were to broaden at the expense of the downward transport without any co-occurrent circulation accelerations, the width term would lead to an amplification of upward transport and weakening of downward transport. The width term also includes situations where a completely new area of upward or downward transport appears in places where there was a continuous region of transport in the opposite direction in the previous time step.

Finally, the method highlights the meridional component of the circulation, which is closely tied to the geometry of the level (the shape term in Equation 7), across which the transport is diagnosed. As can be seen in Equation 1, the $\overline{v}^*$ term contributes to the net transport only in places where the geometry of the zonal mean stratopause is sufficiently slanted. In situations where $\tan\alpha \approx 0$ even a very significant change in the meridional component of the circulation cannot be of great importance for changes in the transport across the stratopause. The shape term contains the temporal changes in the local slopes of the zonal mean stratopause. Its amplitude is more pronounced in places with steeper slopes (due to the factor $\frac{1}{\cos^2\alpha}$) and stronger meridional circulation.

Time series for each term represent the evolution of transport from the starting year 1960 under the isolated influence of the individual mechanism. Additionally, by summing all the terms, we can reconstruct and compare the sum of all the terms of the decomposition with the transport computed directly from the data according to the definition in Equation 1. This enables an easy verification of the accuracy of the decomposition by examining the Pearson correlation between the two (directly computed and reconstructed) series of mass transport across the stratopause. For the application of the decomposition methodology on the annual mean data, the correlation exceeds 0.99 for all models, signifying an excellent accuracy of this decomposition at the leading order.

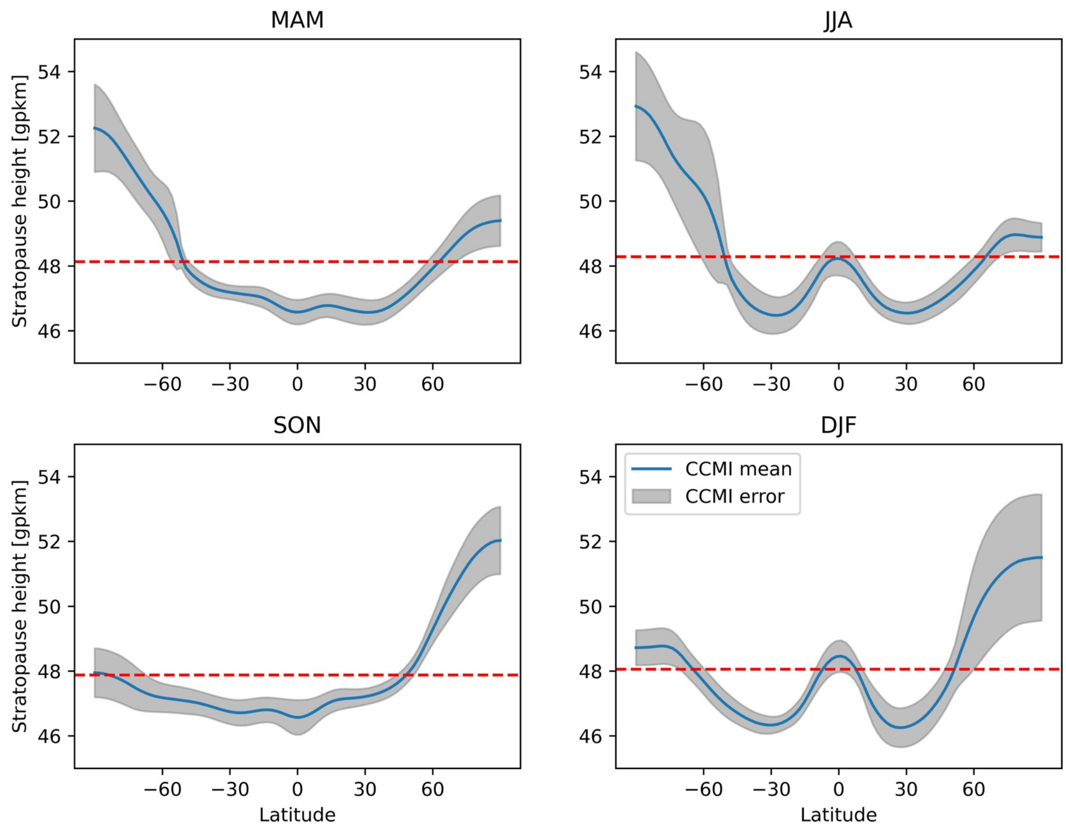

Figure 1. Multi-model mean (blue line) and its standard error (gray shading) of the seasonal climatologies (1960–2000) of the zonal mean stratopause height (in geopotential kilometers) based on monthly mean values. The red line indicates a global mean for a given season. Results for individual models can be seen in the Supplement as Figure S1 in Supporting Information S1.

3. Results

3.1. Climatology, Variability and Trend of the Advective Mass Transport Across the Stratopause

A key factor, alongside the residual mean circulation, affecting the seasonal variability of advective transport between the stratosphere and mesosphere is the annual cycle of the stratopause height and shape. Due to the exponential decrease in density with height, the mass flux across the stratopause is strongly dependent on the actual height of the stratopause. Furthermore, the shape of the stratopause impacts the efficiency of the meridional transport, which can be significant even for small slopes of the stratopause, because the meridional residual mean velocity is of several orders of magnitude larger than the vertical velocity.

Figure 1 shows a meridional climatological distribution of the zonal mean stratopause height for each season using the multi-model mean (MMM) and spread represented by the standard error of the MMM. Although the global mean height of the zonally averaged stratopause is similar for all seasons (about 48 km), its shape changes substantially throughout the year. In general, all the analyzed models reproduce the salient features of the stratopause seasonal (semi-annual oscillation (SAO) pattern in the equatorial region) and latitudinal variability (polar separation) that are known from observations (Barnett, 1974; France & Harvey, 2013; Hitchman & Leovy, 1986; Kawatani et al., 2020; Labitzke, 1974). As a result, qualitatively different shapes of the stratopause are observed during the transition (MAM and SON) and solstice (DJF and JJA) seasons.

The shape of the stratopause during SON and MAM is characterized by a global maximum stratopause height above the upcoming winter pole and a secondary maximum over the upcoming summer pole (not as pronounced during SON in the southern hemisphere). Between the polar regions, the zonal mean stratopause height varies negligibly with latitude, being almost flat. The distribution of inter-model variance is relatively uniform, with slightly higher spread over the poles.

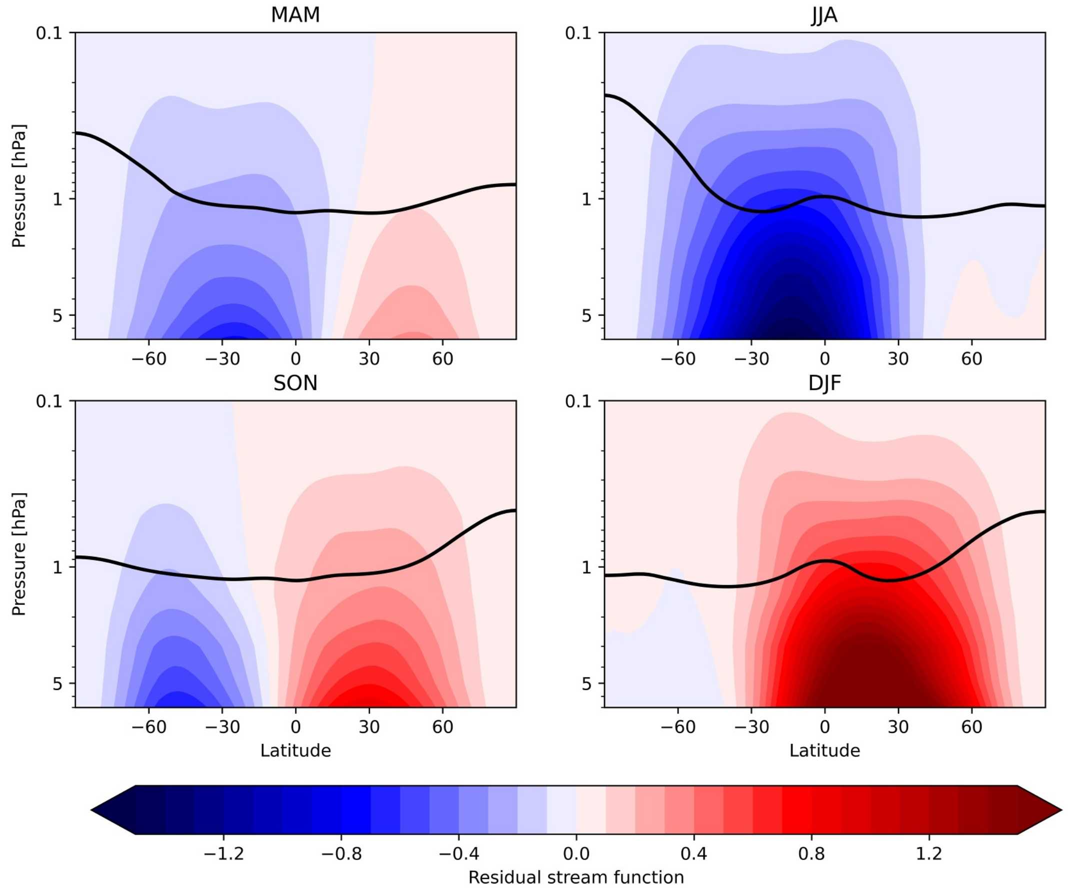

Figure 2. Multi-model mean of the seasonal climatologies (1960–2000) of the residual stream function (in 10^9 kg $\cdot$ s^{-1}) based on monthly mean values. The black solid line indicates the mean stratopause position during the season.

The solstice seasons (DJF and JJA) are characterized by an additional local maximum of the stratopause height in the equatorial region. Hence, the SAO affects the climatological shape of the zonal mean stratopause. If we focus on the standard error of the MMM, we see that it is relatively small for the zonal mean stratopause heights in the equatorial region, but it grows considerably when going poleward (especially towards the winter pole). The polar regions in their respective winters are the areas of highest spread between models, which is likely tied to the inter-model differences in polar vortex strength and frequency of sudden stratospheric warmings (Ayarzagüena et al., 2018). Analogous results for individual models can be found in the Supplement as Figure S1 in Supporting Information S1.

To illustrate the seasonal cycle of the advective part of the BDC in the upper stratosphere and mesosphere in CCMI-1 models, seasonal climatologies of the MMM residual stream function in the upper stratosphere and mesosphere are depicted in Figure 2. The characteristic single-cell circulation from the summer to the winter hemisphere, pronounced during the solstice seasons, is well represented by the MMM mean. During transition seasons, the circulation changes its direction, producing, in a climatological mean, two circulation cells, one in each hemisphere, with one area of upwelling centered in the tropics of the spring hemisphere and with the downwelling regions at higher latitudes.

The position and shape of the zonal mean stratopause, together with the distribution of the residual mean circulation and density, jointly influence the advective mass exchange between stratosphere and mesosphere. The climatological seasonal distribution of the zonal mean advective mass flux across the stratopause (upward transport positive, downward transport negative) for the MMM and its standard error is shown in Figure 3. In the figure, we have highlighted in orange the contribution of the meridional advection to the cross-stratopause transport, which is closely tied to the shape of the stratopause through the angle α (see Equation 1).

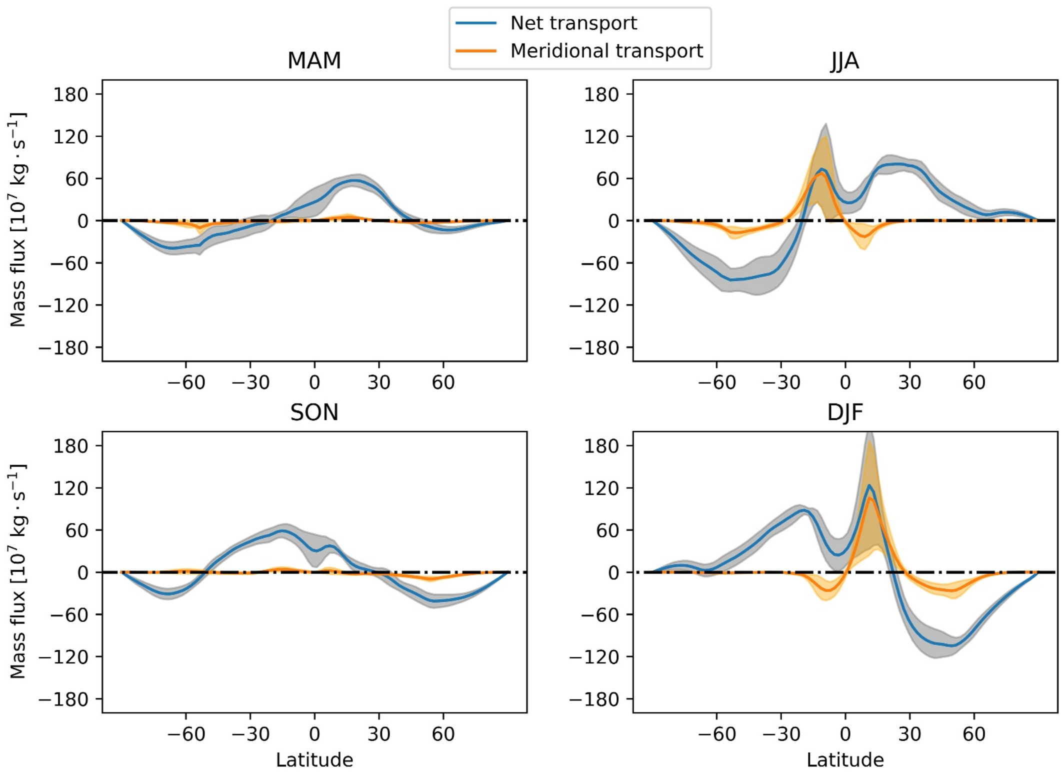

Figure 3. Multi-model mean (blue line) and its standard error (gray shading) of the seasonal climatologies (1960–2000) of the zonal mean advective mass flux across the stratopause (positive sign for flux from stratosphere to mesosphere) based on monthly mean values. The orange color depicts the contribution from the meridional residual mean velocity component.

The seasonality of the net transport across the stratopause largely corresponds with the seasonality of the deep branch of the BDC. The net upward transport (and downward by continuity) is strongest during the solstice seasons (DJF and JJA), associated with the single pole-to-pole circulation from the summer to the winter pole. Locally, except in the polar regions, have shown is also the case for the vertical structure of the stratosphere. The mass flux is stronger in both directions (from and into the stratosphere) during the boreal winter (DJF). Notably, the upward transport exhibits a pronounced two-peak structure in the MMM during both DJF and JJA due to the inclusion of the meridional contribution to the net transport.

Firstly, there is the well-known peak in the summer hemisphere exclusively connected with the vertical mass flux. Secondly, there is an equally strong, narrow peak in the tropics of the winter hemisphere connected with the meridional circulation component and the slope of the stratopause in the region. For DJF, the second peak in the tropics of the winter hemisphere has a slightly higher magnitude in the MMM compared to the peak in the summer hemisphere. However, the strength of the meridional transport in this region is subject to a large spread between the models, contributing to the variability observed in the ensemble. Also, note that at the other side of the tropical region, where the slope of the stratopause is opposite, the meridional advection adds to the downward transport, contributing to the saddle region in the mass flux around the equator in DJF and JJA.

The zonal mean advective mass transport across the stratopause during the transition seasons is weaker, with the upward transport centered in the tropics of the spring hemisphere and downward transport in the extratropics of each hemisphere (in MAM, the downward transpor in the NH is almost non-existent). The meridional component has only a minor contribution during MAM and SON.

By integrating the mass fluxes across the stratopause, shown in Figure 3, we can derive time series of the net upward and downward transport. The climatological annual cycle of the net transport between the stratosphere and mesosphere is illustrated in Figure 4. It shows a pronounced seasonal dependence of the magnitude of advective exchange between stratosphere and mesosphere, with peaks observed during the summer and winter months. During this period, the net advective mass transport roughly doubles compared to the spring and autumn

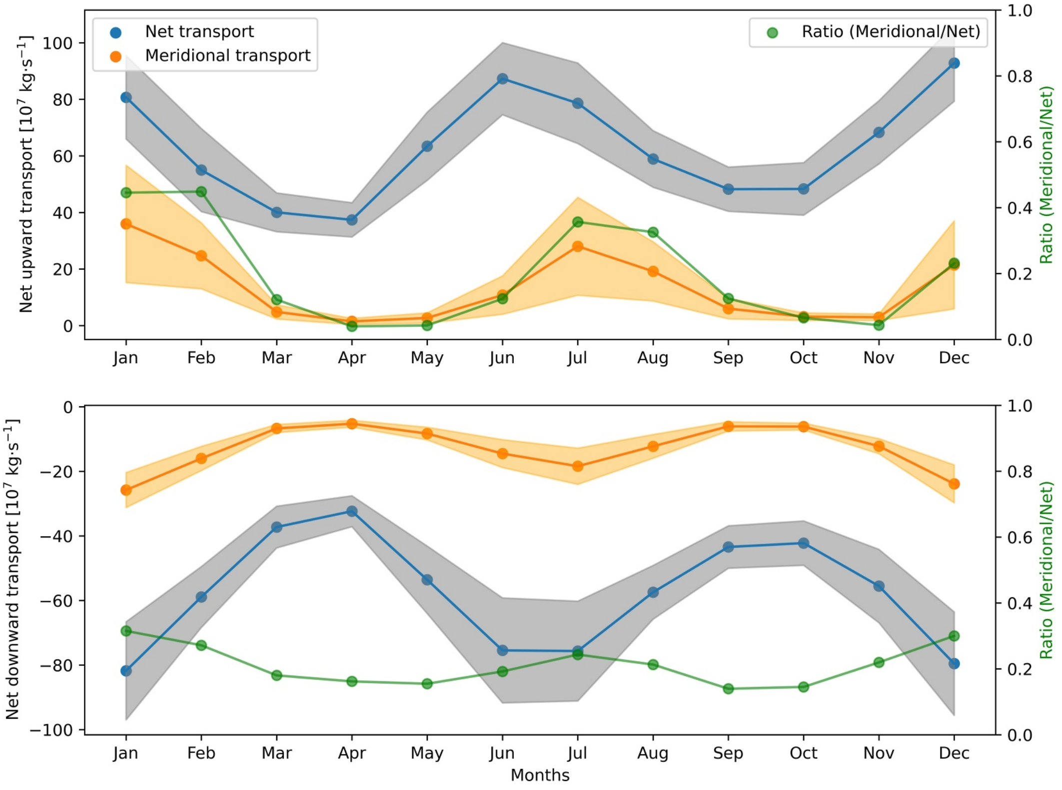

Figure 4. Annual cycle of the net (blue) transport, its meridional component (orange), and ratio between them (green) based on monthly mean data for 1960–2000. Dots represent the multi-model mean (MMM), and the standard error of the MMM is indicated by shading.

months. Especially for upward transport, the meridional component of the transport plays an important role for the seasonal variability, constituting around 40% of the mass flux from the stratosphere to the mesosphere during summer and winter months.

Meridional contribution to the transport from the mesosphere to the stratosphere is responsible for approximately one quarter of the flux, but the ratio is almost constant over the year with only a slight increase during the solstice seasons. This is one of the reasons why the annual cycle has a smaller amplitude for the net downward than for upward transport. However, we must note that there is a considerable spread between the models regarding the meridional transport contribution to the net upward and downward transport during the solstice seasons.

Lin and Fu (2013) showed that the deep branch of the BDC robustly accelerates with increasing GHGs in climate model projections. This is reflected in the 1960–2099 time series of the cross-stratopause net upward (Figure 5) and downward transport (Figure 6) across the stratopause separated in the four seasons. Across all seasons, we diagnose a statistically significant linear trend for both the net upward and downward transport in the MMM, pointing to the increasing advective exchange of mass between stratosphere and mesosphere. On a side note, no pronounced changes in the upward or downward transport time series around the year 2000 (except a slight hint for both parts of transport in DJF) can be seen. This suggests that the advective transport across the stratopause is not sensitive to the reversal of ODS emission trends and the associated ozone recovery, which Pišoft et al. (2021) have shown is also the case for the vertical structure changes in the stratosphere.

The magnitude of the linear trends for MMM is around 1% per decade relative to the 1960–2000 mean mass flux value, with the highest trend values diagnosed in SON for both upward (∼ 1.35%) and downward transport (∼ 1.23%). For all seasons, the relative amplification of upward transport is slightly stronger than that of downwelling, however, this difference is within statistical error.

The robust and statistically significant amplification of transport between the stratosphere and mesosphere for all seasons in the MMM view is also confirmed by the trends for the individual models summarized in Figure 7. A

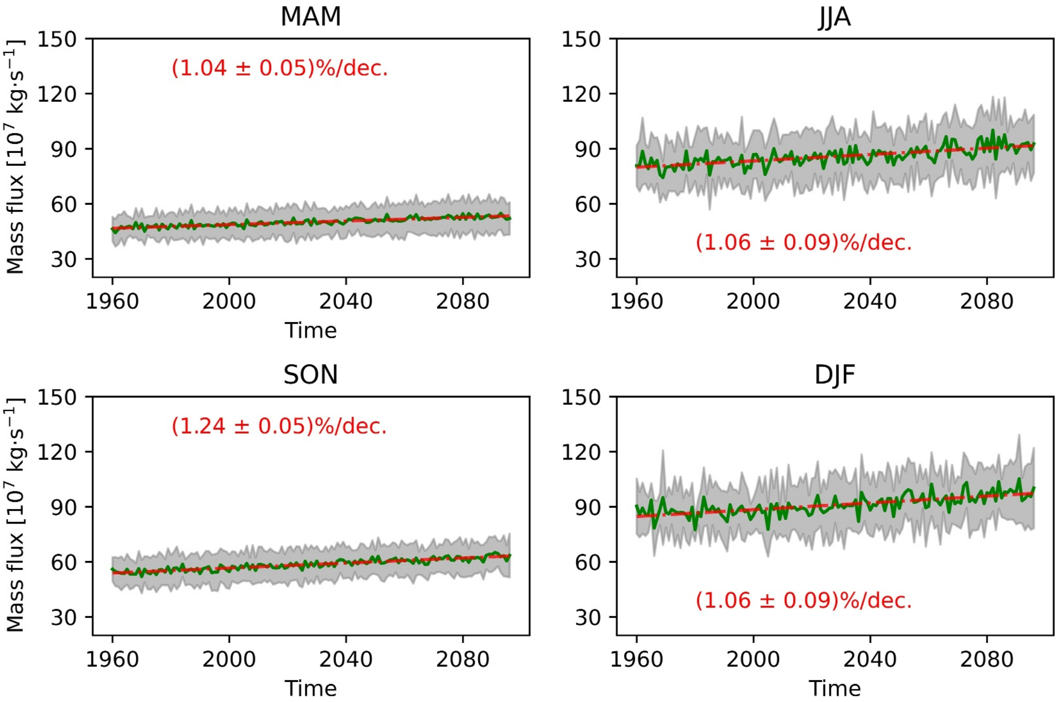

Figure 5. Time evolution of the multi-model mean (MMM) (green solid line), its standard error (gray shading), and MMM linear trend (red dotted line) of net advective transport from the stratosphere to the mesosphere based on monthly mean values. The value of the linear trend is given relative to the 1960–2000 mean value. All marked trends are statistically significant at a confidence level of 95% using the Wald test.

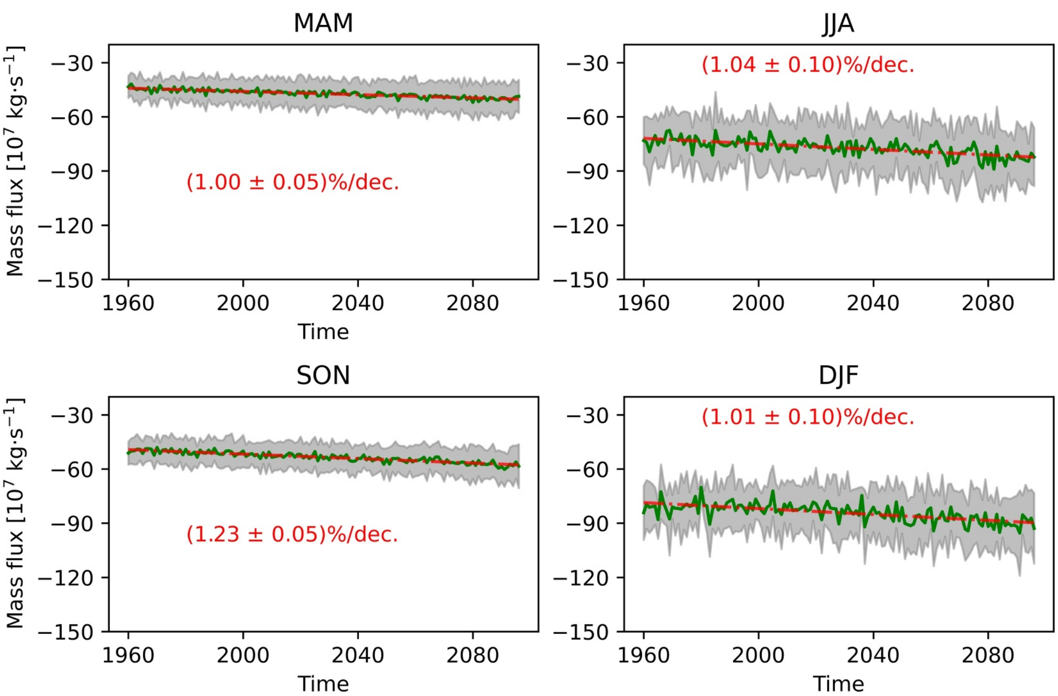

Figure 6. As Figure 5, but for transport from the mesosphere to the stratosphere.

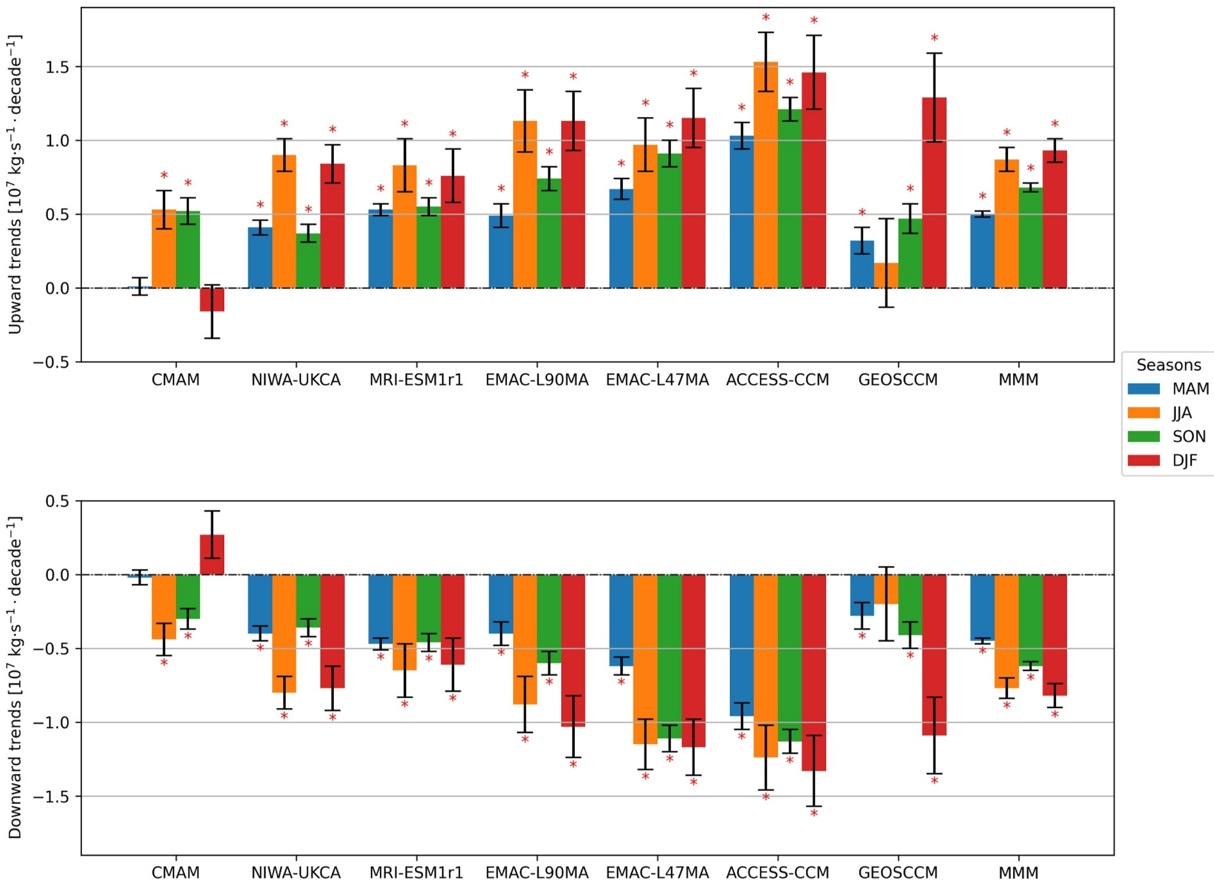

Figure 7. Upward and downward transport trends with standard error represented by error bar using OLS regression for individual models and multi-model mean for 1960–2099. Statistically significant trends at a confidence level of 95% using the Wald test are marked with red asterisk.

significant trend was detected for the vast majority of models and seasons, with the exception of MAM and DJF for CMAM and JJA for GEOSCCM. Comparing the trends for upward and downward transport confirms the expected interdependence and balance between the two transport components, with an increase in upward transport for a given season corresponding to a roughly equal increase in downward transport.

That said, although most models agree on a statistically significant amplification of the stratosphere-mesosphere exchange, the amplitude of the trends for individual models varies considerably in most cases. To better understand the causes of the variability in climatology and projected changes of upward and downward transport among models, the next subsection employs a novel approach to the decomposition of total transport into its individual components in an annual view perspective, detailed in Section 2.3.

3.2. Analyzing the Inter-Model Differences Using the Decomposition Method

In this subsection, we apply the decomposition method to analyze the cross-stratopause transport trends caused by increasing GHG emissions in greater detail. The method allows us to disentangle inter-model differences into their primary mechanisms, thus revealing their reasons.

Due to large shifts in upward and downward transport regions during the year (see Figure 3) and high degree of month-to-month variability in the considered altitudes, accurate application of the decomposition is possible only for annual mean data (see Šácha et al., 2024). Hence, we can apply this analysis only on inter-model comparison of the long-term trends based on the annual mean data.

Figure 8 shows that there is a significant increasing trend (and considerable spread in its magnitude) in both annual mean upward and downward transport. From the decomposition, we see that the upward transport trend is a result of positive contributions from the $\overline{w}^*$, z, and width (widening of the upward transport region) terms, partly

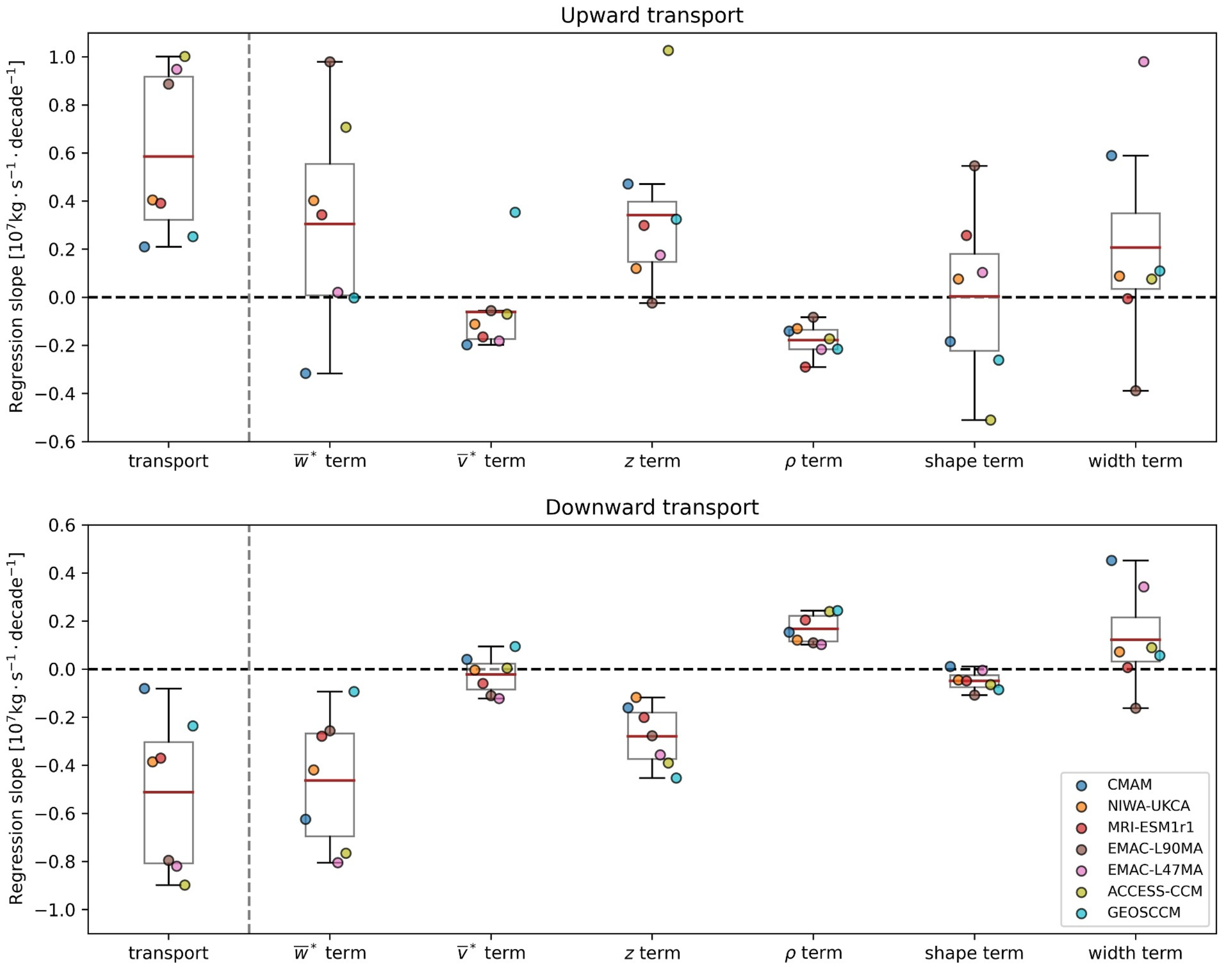

Figure 8. Linear trends based on individual model simulations for net upward and downward transport across the stratopause computed directly (first column, transport) and for the individual terms of the decomposition. The box extends from the first quartile to the third quartile. The whiskers extend from the box to the farthest trend lying within 1.5* the inter-quartile range from the box. The brown lines indicate the multi-model mean trends.

compensated by the $\overline{v}^*$ and ρ terms. The largest spread in the trends are in the $\overline{w}^*$, shape, and width terms, where the spread between the models is higher than for the net trend.

For annual mean downward transport trends, we see negative (strengthening) contributions mainly from the $\overline{w}^*$ and z terms with weaker, counteracting contributions from the ρ and width terms. The spread is dominated by the $\overline{w}^*$ and width terms, but it is much smaller than for the upward transport.

The decomposition reveals an interesting contrast between cross-stratopause transport and upwelling in the shallow BDC branch in general, which was analyzed in Šácha et al. (2024). In the lower stratosphere, the pressure levels and the tropopause are rising, hence the z term is always negative and the net transport is a result of a high degree of compensation between the $\overline{w}^*$ and z terms (Šácha et al., 2024). On the contrary, across the stratopause, the two major terms add up to the net trend of upward and downward transport, leading to stronger trends.

Regarding the inter-model differences in the cross-stratopause transport trends, from Figure 8 we can separate the models into two groups. Namely, the ones that project stronger upwelling trends including both EMAC versions and ACCESS-CCM (around $1 \cdot 10^7$ kg · s^{-1} · decade^{-1}) and the ones projecting weaker trends comprising the rest of the models (around $0.3 \cdot 10^7$ kg · s^{-1} · decade^{-1}). However, the other panels of Figure 8 show that the combination of individual mechanisms contributing to the trend is different between all the models. Even for EMAC-L47 and EMAC-L90, which differ only by their vertical resolution, the analysis reveals considerable differences in the contribution from the mechanisms, most pronounced for the $\overline{w}^*$ term and for the widening term. The net upward transport trend of these two realizations, however, is very similar. Dedicated experiments varying vertical and horizontal model resolution systematically could shed more light on the impact of these parameters for cross-stratopause transport in general and for the individual contributions in particular.

Among the models, CMAM projects the smallest net upward transport trend. This can be attributed to negative trends observed in both the meridional and vertical components of the residual mean circulation terms, although these components exhibit considerably non-linear behavior. However, despite the circulation deceleration in CMAM, the slightly positive net upward transport trend is sustained by substantial contributions from the vertical shift and widening terms.

The models exhibit the strongest agreement in two aspects: the contribution from the trend of the density term and the sign of the trend associated with the vertical shift with the exception of EMAC-L90, whose trend in z term is almost zero. This consistency suggests that the models align most closely in projecting changes directly related to radiative processes.

The most significant variations between the models arise from changes in circulation, horizontal structure (width of the upwelling region), and the shape of the stratopause. Except for GEOS, there is notable agreement in the contribution to the trend from the meridional circulation term. However, due to disparities in the shape term that governs the efficiency of the meridional circulation term for cross-stratopause transport, its overall impact remains highly uncertain.

For the net downward transport trend, the two groups of models can again easily be identified by the magnitude of the trend, as for the net upward transport. The models with stronger trends this time agree better on the individual factors contributing to the downwelling trend. In particular, the big spread in the term connected with the vertical shift, as seen for the upwelling, is now diminished. However, notable differences persist in the contributions from the $\overline{w}^*$ and widening terms.

The overall analysis of the downward transport trends in all the models indicates that the $\overline{v}^*$ and shape-related terms have a minor impact. The models exhibit the highest level of agreement regarding the contributions from the vertical shift and density terms, which also align well with the linear model. However, the largest variations are observed in the $\overline{w}^*$ and widening terms, where EMAC-L47 and EMAC-L90 show significant disparities. The decomposition analysis clarifies the reason behind the smallest downward transport trend observed in CMAM, which is attributed to the pronounced narrowing of the downwelling region in that particular model.

Finally, we note that not only do the individual models differ in their projections of the long-term evolution of contributing mechanisms, but also the relationships between these individual mechanisms vary across models. This is extensively quantified by the inter-term correlations provided for each model in the Supplement (Figures S2 and S3 in Supporting Information S1). For example, the correlation between the $\overline{v}^*$ terms and shape terms fluctuates between strongly positive (in the case of CMAM), weakly positive (ACCESS), weakly negative (GEOSCCM and both EMAC versions), and strongly negative (NIWA-UKCA and MRI-ESM). These variations suggest completely different interactions between the circulation and horizontal structure changes at the stratopause heights among the models. Furthermore, it should be noted that the relationships between individual terms significantly differ in terms of strength and the sign of correlation even among the two different configurations of the EMAC model.

4. Summary and Conclusions

In the presented study, we have analyzed the climatology of the advective transport between the stratosphere and mesosphere and its response to changes in GHG emissions using a set of chemistry-climate model projections. The distribution of upward and downward transport regions has a well-known seasonal dependence, and the strength of the advective transport is greater during the solstice seasons than during the transition seasons. As a novel finding, we report a pronounced two-peak structure of the upwelling from the stratosphere to the mesosphere during solstice seasons, with the well-known peak of the transport from the stratosphere to the mesosphere in the summer hemisphere that is exclusively connected with the upward mass flux, and a second narrow peak in the tropics of the winter hemisphere that is due to the meridional circulation component and the slope of the stratopause that allows the meridional circulation component to contribute to advective cross-stratopause transport.

Our study focuses solely on the advective component of transport, which can be computed using the residual mean circulation. However, transport can also occur through (quasi-)isentropic mixing (e.g., Dietmüller et al., 2017; Eichinger et al., 2019), as the stratopause is not a strict transport barrier. Due to the relative positioning of the stratopause to isentropic surfaces (see Figure S4 in Supporting Information S1), significant mixing contributions to the mass exchange can be expected, particularly in the winter hemisphere. Potential future changes in mixing within the upper stratosphere and mesosphere remain largely unexplored, which calls for further investigation.

For both directions of the advective transport between the stratosphere and mesosphere, the models show a clear and statistically significant increasing trend for the annual mean data and seasonal means. The absence of any trend break around the year 2000 suggests a negligible role of ODSs and ozone compared to GHGs in driving the trend. Both in the climatology and the long-term evolution of the net upward and downward transport, we have found a large spread between individual model simulations, which motivated us to produce a detailed analysis of the underlying mechanisms that contribute to the net upwelling and downwelling trends. The decomposition into individual contributions reveals that all mechanisms induced by the increasing GHG emissions (accelerating flow, vertical and horizontal structure changes) significantly influence the MMM trend for both upward and downward transport. However, the models largely disagree on the strength and mostly also on the direction of these contributions. For the net upward transport, the models only agree on the contribution from the density changes. For the downward transport, the spread is almost exclusively due to differences in the term connected with the vertical residual mean velocity component and with the changes in the width (predominantly narrowing) of the region, where the air crosses the stratopause from the mesosphere to the stratosphere.

Overall, we have made a first research effort to study advective transport between the stratosphere and mesosphere. For quantifying the exchange, we have chosen the thermally determined stratopause, as a natural candidate for the level across which the transport is diagnosed. However, the stratopause is not a transport barrier and its location can be also non-linearly dependent on the strength of the circulation. We assume that studies targeting specific phenomena affected by the transport between the stratosphere and mesosphere will have to define specific regions of interests beyond the general stratosphere-mesosphere classification used in our study. For instance, mesospheric phenomena connected with solar radiation (SF_6 sinks, NO_x) tend to be linked with constant altitude regions, in contrast to meteor and debris studies concerned with constant density levels, which will be shifting downwards in the course of climate change (Eichinger & Šácha, 2020; Mlynczak et al., 2022; Pišoft et al., 2021). Quantification of transport relevant for each of these impacts will have to be computed separately then, evaluating the transport across case-specific levels.

Regardless of the level where we diagnose it, our results demonstrate that projecting the changes in mean meridional overturning circulation in the upper stratosphere and mesosphere is a highly complex task for the models because they have to capture not only the circulation changes but also the co-occurring changes in the vertical and horizontal structure of the atmosphere that can be possibly non-linearly related. The high susceptibility of the resulting trends to even small nuances in the model formulation is underlined by the completely different results of the decomposition for two model simulations that differ only in their vertical resolution (EMAC-L47 and EMAC-L90).

The strong agreement among models in the primarily radiatively driven density and z terms suggests that variations in radiative transfer schemes or chemistry between models have only small influence on the differences observed in net transport trends. This implies that other factors likely contribute more considerably to the discrepancies in transport. For instance, it has been shown that differences in the parameterized orographic gravity wave drag in CMIP6 models project into the climatological differences of the dynamics in the stratosphere between the models (Hájková & Šácha, 2023), with a possibly even larger role of the non-orographic gravity wave parameterizations in the upper stratosphere and mesosphere of the models.

Finally, although there are some observational constraints on the upper BDC branch based on long-lived trace gases such as CFCs, CH_4, and H_2O, these observations are limited and lack a longer record. Therefore, the decomposition may prove useful in highlighting the mechanisms that are linked to the transport changes but are easier to constrain. This is the case especially for the vertical and horizontal structure changes of the region that were shown to have a considerable impact on the projected transport trends and that can be constrained by satellite observations, subject to the availability of sufficiently homogeneous and stable data records from the missions.

Data Availability Statement

All CCMI-1 data used in this study can be obtained through the British Atmospheric Data Centre (BADC) archive (https://archive.ceda.ac.uk; accessed 1 February 2020). Transport and decomposition time series were published in Zajíček (2023).

Acknowledgments

We would like to thank the reviewers and the editor for helping us to improve the manuscript during the review process. Funding: Czech Science Foundation JUNIOR-STAR Grant 23-04921M; Czech Science Foundation Grant 21-03295S; Charles University, project GA UK 456622. Charles University Research Centre Program UNCE/24/SCI/005. Petr Pišoft and Jiří Mikšovský were supported by the Johannes Amos Comenius Programme (P JAC) project CZ.02.01.01/00/22_008/0004605, Natural and anthropogenic georisks. Open access publishing facilitated by Univerzita Karlova, as part of the Wiley - CzechELib agreement.

References

Abalos, M., Calvo, N., Benito-Barca, S., Garny, H., Hardiman, S. C., Lin, P., et al. (2021). The Brewer–Dobson circulation in CMIP6. *Atmospheric Chemistry and Physics*, *21*(17), 13571–13591. https://doi.org/10.5194/acp-21-13571-2021

Andersson, M. E., Verronen, P. T., Marsh, D. R., Seppälä, A., Päivärinta, S.-M., Rodger, C. J., et al. (2018). Polar ozone response to energetic particle precipitation over decadal time scales: The role of medium-energy electrons. *Journal of Geophysical Research: Atmospheres*, *123*(1), 607–622. https://doi.org/10.1002/2017JD027605

Andrews, D. G., Holton, J. R., & Leovy, C. B. (1987). *Middle atmosphere dynamics*. Academic Press.

Ayarzagüena, B., Polvani, L. M., Langematz, U., Akiyoshi, H., Bekki, S., Butchart, N., et al. (2018). No robust evidence of future changes in major stratospheric sudden warmings: A multi-model assessment from CCMI. *Atmospheric Chemistry and Physics*, *18*(15), 11277–11287. https://doi.org/10.5194/acp-18-11277-2018

Ball, W. T., Alsing, J., Mortlock, D. J., Rozanov, E. V., Tummon, F., & Haigh, J. D. (2017). Reconciling differences in stratospheric ozone composites. *Atmospheric Chemistry and Physics*, *17*(20), 12269–12302. https://doi.org/10.5194/acp-17-12269-2017

Barnett, J. J. (1974). The mean meridional temperature behaviour of the stratosphere from November 1970 to November 1971 derived from measurements by the selective chopper radiometer on nimbus IV. *Quarterly Journal of the Royal Meteorological Society*, *100*(426), 505–530. https://doi.org/10.1002/qj.49710042602

Berger, U., & Lübken, F.-J. (2011). Mesospheric temperature trends at mid-latitudes in summer. *Geophysical Research Letters*, *38*(22), L22804. https://doi.org/10.1029/2011GL049528

Birner, T., & Bönisch, H. (2011). Residual circulation trajectories and transit times into the extratropical lowermost stratosphere. *Atmospheric Chemistry and Physics*, *11*(2), 817–827. https://doi.org/10.5194/acp-11-817-2011

Brewer, A. W. (1949). Evidence for a world circulation provided by the measurements of helium and water vapour distribution in the stratosphere. *Quarterly Journal of the Royal Meteorological Society*, *75*(326), 351–363. https://doi.org/10.1002/qj.49707532603

Brinkop, S., Dameris, M., Jöckel, P., Garny, H., Lossow, S., & Stiller, G. (2016). The millennium water vapour drop in chemistry–climate model simulations. *Atmospheric Chemistry and Physics*, *16*(13), 8125–8140. https://doi.org/10.5194/acp-16-8125-2016

Butchart, N. (2014). The Brewer-Dobson circulation. *Reviews of Geophysics*, *52*(2), 157–184. https://doi.org/10.1002/2013RG000448

D'Ambrosio, A., Lifson, M., Jang, D., Pasiecznik, C., & Linares, R. (2022). Projected orbital demand and leo environmental capacity.

Deushi, M., & Shibata, K. (2011). Development of a meteorological research institute chemistry-climate model version 2 for the study of tropospheric and stratospheric chemistry. *Papers in Meteorology and Geophysics*, *62*, 1–46. https://doi.org/10.2467/mripapers.62.1

Dietmüller, S., Garny, H., Plöger, F., Jöckel, P., & Cai, D. (2017). Effects of mixing on resolved and unresolved scales on stratospheric age of air. *Atmospheric Chemistry and Physics*, *17*(12), 7703–7719. https://doi.org/10.5194/acp-17-7703-2017

Dobson, G. M. B., Harrison, D. N., & Lawrence, J. (1929). Measurements of the amount of ozone in the earth's atmosphere and its relation to other geophysical conditions.—Part III. *Proceedings of the Royal Society of London - Series A: Containing Papers of a Mathematical and Physical Character*, *122*(790), 456–486. https://doi.org/10.1098/rspa.1929.0034

Eichinger, R., Dietmüller, S., Garny, H., Šácha, P., Birner, T., Bönisch, H., et al. (2019). The influence of mixing on the stratospheric age of air changes in the 21st century. *Atmospheric Chemistry and Physics*, *19*(2), 921–940. https://doi.org/10.5194/acp-19-921-2019

Eichinger, R., & Šácha, P. (2020). Overestimated acceleration of the advective Brewer–Dobson circulation due to stratospheric cooling. *Quarterly Journal of the Royal Meteorological Society*, *146*(733), 3850–3864. https://doi.org/10.1002/qj.3876

France, J. A., & Harvey, V. L. (2013). A climatology of the stratopause in WACCM and the zonally asymmetric elevated stratopause. *Journal of Geophysical Research: Atmospheres*, *118*(5), 2241–2254. https://doi.org/10.1002/jgrd.50218

Garcia, R. R. (2021). On the response of the middle atmosphere to anthropogenic forcing. *Annals of the New York Academy of Sciences*, *1504*(1), 25–43. https://doi.org/10.1111/nyas.14664

Garny, H., Birner, T., Bönisch, H., & Bunzel, F. (2014). The effects of mixing on age of air. *Journal of Geophysical Research: Atmospheres*, *119*(12), 7015–7034. https://doi.org/10.1002/2013jd021417

Garny, H., Eichinger, R., Laube, J. C., Ray, E. A., Stiller, G. P., Bönisch, H., et al. (2024). Correction of stratospheric age of air (AOA) derived from sulfur hexafluoride (sf_6) for the effect of chemical sinks. *Atmospheric Chemistry and Physics*, *24*(7), 4193–4215. https://doi.org/10.5194/acp-24-4193-2024

Granier, C., Bessagnet, B., Bond, T., D'Angiola, A., Denier van der Gon, H., Frost, G., et al. (2011). Evolution of anthropogenic and biomass burning emissions of air pollutants at global and regional scales during the 1980–2010 period. *Climatic Change*, *109*(1–2), 163–190. https://doi.org/10.1007/s10584-011-0154-1

Hájková, D., & Šácha, P. (2023). Parameterized orographic gravity wave drag and dynamical effects in CMIP6 models. *Climate Dynamics*, *62*(3), 1–26. https://doi.org/10.1007/s00382-023-07021-0

Hardiman, S. C., Butchart, N., & Calvo, N. (2014). The morphology of the Brewer–Dobson circulation and its response to climate change in CMIP5 simulations. *Quarterly Journal of the Royal Meteorological Society*, *140*(683), 1958–1965. https://doi.org/10.1002/qj.2258

Hitchman, M. H., & Leovy, C. B. (1986). Evolution of the zonal mean state in the equatorial middle atmosphere during October 1978–May 1979. *Journal of the Atmospheric Sciences*, *43*(24), 3159–3176. https://doi.org/10.1175/1520-0469(1986)043⟨3159:EOTZMS⟩2.0.CO;2

IPCC. (2023). *Climate change 2021 – the physical science basis: Working group i contribution to the sixth assessment report of the intergovernmental panel on climate change*. Cambridge University Press.

Jackman, C. H., Marsh, D. R., Vitt, F. M., Garcia, R. R., Fleming, E. L., Labow, G. J., et al. (2008). Short- and medium-term atmospheric constituent effects of very large solar proton events. *Atmospheric Chemistry and Physics*, *8*(3), 765–785. https://doi.org/10.5194/acp-8-765-2008

Jöckel, P., Kerkweg, A., Pozzer, A., Sander, R., Tost, H., Riede, H., et al. (2010). Development cycle 2 of the modular earth submodel system (MESSy2). *Geoscientific Model Development*, *3*(2), 717–752. https://doi.org/10.5194/gmd-3-717-2010

Jöckel, P., Tost, H., Pozzer, A., Kunze, M., Kirner, O., Brenninkmeijer, C. A. M., et al. (2016). Earth system chemistry integrated modelling (ESCIMO) with the modular earth submodel system (MESSY) version 2.51. *Geoscientific Model Development*, *9*(3), 1153–1200. https://doi.org/10.5194/gmd-9-1153-2016

Jonsson, A. I., de Grandpré, J., Fomichev, V. I., McConnell, J. C., & Beagley, S. R. (2004). Doubled CO2-induced cooling in the middle atmosphere: Photochemical analysis of the ozone radiative feedback. *Journal of Geophysical Research*, *109*(D24), D24103. https://doi.org/10.1029/2004JD005093

Karlsson, B., Körnich, H., & Gumbel, J. (2007). Evidence for interhemispheric stratosphere-mesosphere coupling derived from noctilucent cloud properties. *Geophysical Research Letters*, *34*(16), L16806. https://doi.org/10.1029/2007GL030282

Kawatani, Y., Hirooka, T., Hamilton, K., Smith, A. K., & Fujiwara, M. (2020). Representation of the equatorial stratopause semiannual oscillation in global atmospheric reanalyses. *Atmospheric Chemistry and Physics*, *20*(14), 9115–9133. https://doi.org/10.5194/acp-20-9115-2020

Labitzke, K. (1974). The temperature in the upper stratosphere: Differences between hemispheres. *Journal of Geophysical Research (1896-1977)*, *79*(15), 2171–2175. https://doi.org/10.1029/JC079i015p02171

Laštovička, J. (2006). Forcing of the ionosphere by waves from below. *Journal of Atmospheric and Solar-Terrestrial Physics*, *68*(3), 479–497. https://doi.org/10.1016/j.jastp.2005.01.018

Lin, P., & Fu, Q. (2013). Changes in various branches of the brewer–dobson circulation from an ensemble of chemistry climate models. *Journal of Geophysical Research: Atmospheres*, *118*(1), 73–84. https://doi.org/10.1029/2012JD018813

Loeffel, S., Eichinger, R., Garny, H., Reddmann, T., Fritsch, F., Versick, S., et al. (2022). The impact of sulfur hexafluoride sinks on age of air climatologies and trends. *Atmospheric Chemistry and Physics*, *22*(2), 1175–1193. https://doi.org/10.5194/acp-22-1175-2022

Meinshausen, M., Smith, S., Calvin, K., Daniel, J., Kainuma, M., Lamarque, J.-F., et al. (2011). The RCP greenhouse gas concentrations and their extensions from 1765 to 2300. *Climatic Change*, *109*(1–2), 213–241. https://doi.org/10.1007/s10584-011-0156-z

Mlynczak, M. G., Hunt, L. A., Garcia, R. R., Harvey, V. L., Marshall, B. T., Yue, J., et al. (2022). Cooling and contraction of the mesosphere and lower thermosphere from 2002 to 2021. *Journal of Geophysical Research: Atmospheres*, *127*(22), e2022JD036767. https://doi.org/10.1029/2022JD036767

Molod, A., Takacs, L., Suarez, M., & Bacmeister, J. (2015). Development of the geos-5 atmospheric general circulation model: Evolution from MERRA to MERRA2. *Geoscientific Model Development*, *8*(5), 1339–1356. https://doi.org/10.5194/gmd-8-1339-2015

Molod, A., Takacs, L., Suarez, M., Bacmeister, J., Song, I., & Eichmann, A. (2012). The GEOS-5 atmospheric general circulation model: Mean climate and development from MERRA to Fortuna. *Technical Report Series on Global Modeling and Data Assimilation*, *28*, 124. Retrieved from https://gmao.gsfc.nasa.gov/pubs/docs/tm28.pdf

Morgenstern, O., Braesicke, P., O'Connor, F. M., Bushell, A. C., Johnson, C. E., Osprey, S. M., & Pyle, J. A. (2009). Evaluation of the new UKCA climate-composition model – Part 1: The stratosphere. *Geoscientific Model Development*, *2*(1), 43–57. https://doi.org/10.5194/gmd-2-43-2009

Morgenstern, O., Hegglin, M. I., Rozanov, E., O'Connor, F. M., Abraham, N. L., Akiyoshi, H., et al. (2017). Review of the global models used within phase 1 of the chemistry-climate model initiative (CCMI). *Geoscientific Model Development*, *10*(2), 639–671. https://doi.org/10.5194/gmd-10-639-2017

Morgenstern, O., Zeng, G. L., Abraham, N., Telford, P. J., Braesicke, P., Pyle, J. A., et al. (2013). Impacts of climate change, ozone recovery, and increasing methane on surface ozone and the tropospheric oxidizing capacity. *Journal of Geophysical Research: Atmospheres*, *118*(2), 1028–1041. https://doi.org/10.1029/2012jd018382

Oberländer-Hayn, S., Gerber, E. P., Abalichin, J., Akiyoshi, H., Kerschbaumer, A., Kubin, A., et al. (2016). Is the Brewer-Dobson circulation increasing or moving upward? *Geophysical Research Letters*, *43*(4), 1772–1779. https://doi.org/10.1002/2015GL067545

Olivero, J. J., & Thomas, G. E. (1986). Climatology of polar mesospheric clouds. *Journal of the Atmospheric Sciences*, *43*(12), 1263–1274. https://doi.org/10.1175/1520-0469(1986)043⟨1263:COPMC⟩2.0.CO;2

Oman, L. D., Douglass, A. R., Ziemke, J. R., Rodriguez, J. M., Waugh, D. W., & Nielsen, J. E. (2013). The ozone response to ENSO in aura satellite measurements and a chemistry-climate simulation. *Journal of Geophysical Research: Atmospheres*, *118*(2), 965–976. https://doi.org/10.1029/2012JD018546

Oman, L. D., Ziemke, J. R., Douglass, A. R., Waugh, D. W., Lang, C., Rodriguez, J. M., & Nielsen, J. E. (2011). The response of tropical tropospheric ozone to ENSO. *Geophysical Research Letters*, *38*(13), L13706. https://doi.org/10.1029/2011GL047865

Orsolini, Y. J., Limpasuvan, V., Pérot, K., Espy, P., Hibbins, R., Lossow, S., et al. (2017). Modelling the descent of nitric oxide during the elevated stratopause event of January 2013. *Journal of Atmospheric and Solar-Terrestrial Physics*, *155*, 50–61. https://doi.org/10.1016/j.jastp.2017.01.006

Palmeiro, F. M., Calvo, N., & Garcia, R. R. (2014). Future changes in the Brewer–Dobson circulation under different greenhouse gas concentrations in WACCM4. *Journal of the Atmospheric Sciences*, *71*(8), 2962–2975. https://doi.org/10.1175/JAS-D-13-0289.1

Pišoft, P., Šácha, P., Polvani, L. M., Añel, J. A., de la Torre, L., Eichinger, R., et al. (2021). Stratospheric contraction caused by increasing greenhouse gases. *Environmental Research Letters*, *16*(6), 064038. https://doi.org/10.1088/1748-9326/abfe2b

Plane, J. M. C., Feng, W., & Dawkins, E. C. M. (2015). The mesosphere and metals: Chemistry and changes. *Chemical reviews*, *115*(10), 4497–4541. https://doi.org/10.1021/cr500501m

Plumb, R. A. (2002). Stratospheric transport. *Journal of the Meteorological Society of Japan Series II*, *80*(4B), 793–809. https://doi.org/10.2151/jmsj.80.793

Ray, E. A., Moore, F. L., Elkins, J. W., Rosenlof, K. H., Laube, J. C., Röckmann, T., et al. (2017). Quantification of the sf6 lifetime based on mesospheric loss measured in the stratospheric polar vortex. *Journal of Geophysical Research: Atmospheres*, *122*(8), 4626–4638. https://doi.org/10.1002/2016JD026198

Šácha, P., Eichinger, R., Garny, H., Pišoft, P., Dietmüller, S., de la Torre, L., et al. (2019). Extratropical age of air trends and causative factors in climate projection simulations. *Atmospheric Chemistry and Physics*, *19*(11), 7627–7647. https://doi.org/10.5194/acp-19-7627-2019

Šácha, P., Zajíček, R., Kuchař, A., Eichinger, R., Pišoft, P., & Rieder, H. E. (2024). Disentangling the advective Brewer-Dobson circulation change. *Geophysical Research Letters*, *51*(12), e2023GL105919. https://doi.org/10.1029/2023GL105919

Santer, B. D., Sausen, R., Wigley, T. M. L., Boyle, J. S., AchutaRao, K., Doutriaux, C., et al. (2003). Behavior of tropopause height and atmospheric temperature in models, reanalyses, and observations: Decadal changes. *Journal of Geophysical Research*, *108*(D1), 4002. https://doi.org/10.1029/2002JD002258

Scinocca, J. F., McFarlane, N. A., Lazare, M., Li, J., & Plummer, D. (2008). Technical note: The CCCMA third generation AGCM and its extension into the middle atmosphere. *Atmospheric Chemistry and Physics*, *8*(23), 7055–7074. https://doi.org/10.5194/acp-8-7055-2008

Shepherd, T. G., & McLandress, C. (2011). A robust mechanism for strengthening of the Brewer–Dobson circulation in response to climate change: Critical-layer control of subtropical wave breaking. *Journal of the Atmospheric Sciences*, *68*(4), 784–797. https://doi.org/10.1175/2010JAS3608.1

Smith, A. K. (2012). Global dynamics of the MLT. *Surveys in Geophysics*, *33*(6), 1177–1230. https://doi.org/10.1007/s10712-012-9196-9

Smith, A. K., Pedatella, N. M., & Bardeen, C. G. (2022). Global middle-atmosphere response to winter stratospheric variability in saber and MLS mean temperature. *Journal of the Atmospheric Sciences*, *79*(6), 1727–1741. https://doi.org/10.1175/JAS-D-21-0259.1

Smith, A. K., Pedatella, N. M., & Mullen, Z. K. (2020). Interhemispheric coupling mechanisms in the middle atmosphere of WACCM6. *Journal of the Atmospheric Sciences*, *77*(3), 1101–1118. https://doi.org/10.1175/JAS-D-19-0253.1

Solomon, S., Rosenlof, K. H., Portmann, R. W., Daniel, J. S., Davis, S. M., Sanford, T. J., & Plattner, G.-K. (2010). Contributions of stratospheric water vapor to decadal changes in the rate of global warming. *Science*, *327*(5970), 1219–1223. https://doi.org/10.1126/science.1182488

Staten, P., Lu, J., Grise, K., Davis, S., & Birner, T. (2018). Re-examining tropical expansion. *Nature Climate Change*, *8*(9), 768–775. https://doi.org/10.1038/s41558-018-0246-2

Steinbrecht, W., Froidevaux, L., Fuller, R., Wang, R., Anderson, J., Roth, C., et al. (2017). An update on ozone profile trends for the period 2000 to 2016. *Atmospheric Chemistry and Physics*, *17*(17), 10675–10690. https://doi.org/10.5194/acp-17-10675-2017

Stiller, G. P., Fierli, F., Ploeger, F., Cagnazzo, C., Funke, B., Haenel, F. J., et al. (2017). Shift of subtropical transport barriers explains observed hemispheric asymmetry of decadal trends of age of air. *Atmospheric Chemistry and Physics*, *17*(18), 11177–11192. https://doi.org/10.5194/acp-17-11177-2017

Stone, K. A., Morgenstern, O., Karoly, D. J., Klekociuk, A. R., French, W. J., Abraham, N. L., & Schofield, R. (2016). Evaluation of the access – Chemistry–climate model for the southern hemisphere. *Atmospheric Chemistry and Physics*, *16*(4), 2401–2415. https://doi.org/10.5194/acp-16-2401-2016

Thomas, G. E. (1991). Mesospheric clouds and the physics of the mesopause region. *Reviews of Geophysics*, *29*(4), 553–575. https://doi.org/10.1029/91RG01604

World Meteorological Organization. (2011). Scientific assessment of ozone depletion: 2010. Geneva, Switzerland: Global ozone research and monitoring project-report No. 52 (p. 516).

Yukimoto, S., Adachi, Y., Hosaka, M., Sakami, T., Yoshimura, H., Hirabara, M., et al. (2012). A new global climate model of the meteorological research institute: MRI-CGCM3 —Model description and basic performance. *Journal of the Meteorological Society of Japan Series II*, *90A*(0), 23–64. https://doi.org/10.2151/jmsj.2012-A02

Zajíček, R. (2023). Transport between stratosphere and mesosphere datasets. *Zenodo*. https://doi.org/10.5281/zenodo.7956209